Automated Parallel Electrical Characterization of Cells Using Optically-Induced Dielectrophoresis

Na Liu, Yanbin Lin, Yan Peng, Liming Xin, Tao Yue, Yuanyuan Liu, Changhai Ru, Shaorong Xie,
Liang Dong, Huayan Pu, Haige Chen, Wen J. Li, *Fellow, IEEE*, and Yu Sun, *Fellow, IEEE*

Abstract— This article reports an automated optically-induced dielectrophoresis (ODEP) system for characterizing the specific membrane capacitance (SMC) of individual cells. The simulation of cell motion is conducted to analyze the electrokinetic forces acting on the cell. A self-developed visual tracking algorithm for multicells is used to realize an automated process for determining the frequency-sweeping range, crossover frequencies, and cell radii. The SMC values of malignant bladder cancer cells (T24 and RT4) and normal urothelial cells (SV-HUC-1) were quantified using the automated system, demonstrating that the system has a measurement speed of ∼1 cell/s, an accuracy of 1 kHz for the crossover frequency determination, and an accuracy of 0.2 μm for the cell radius measurement.

Note to Practitioners—The current manual optically-induced dielectrophoresis (ODEP) quantification of the specific membrane capacitance (SMC) values of the cells requires a tedious and time-consuming procedure for measuring the cell size and crossover frequency. The automated ODEP approach presented in this article was developed to identify multiple cells and trigger alternating current (ac) bias potential for measuring the radius

Na Liu, Yanbin Lin, Yan Peng, Tao Yue, Yuanyuan Liu, and Huayan Pu are with the School of Mechatronics Engineering and Automation, Shanghai University, Shanghai 200444, China (e-mail: liuna_sia@shu.edu.cn; phygood_2001@shu.edu.cn).

Liming Xin is with the School of Mechatronics Engineering and Automation, Shanghai University, Shanghai 200444, China, and also with the Department of Mechanical and Industrial Engineering, University of Toronto, Toronto, ON M5S 3G8, Canada.

Changhai Ru is with the Research Center of Robotics and Micro System, Soochow University, Suzhou 215021, China, and also with the Collaborative Innovation Center of Suzhou NanoScience and Technology, Soochow University, Suzhou 215021, China.

Shaorong Xie is with the School of Computer Engineering and Science, Shanghai University, Shanghai 200444, China.

Liang Dong and Haige Chen are with the Department of Urology, School of Medicine, Renji Hospital, Shanghai Jiao Tong University, Shanghai 200240, China (e-mail: drdongliang@126.com).

Wen J. Li is with the Department of Mechanical Engineering, City University of Hong Kong, Hong Kong (e-mail: wenjli@cityu.edu.hk).

Yu Sun is with the Department of Mechanical and Industrial Engineering, University of Toronto, Toronto, ON M5S 3G8, Canada (e-mail: sun@mie.utoronto.ca).

This article has supplementary downloadable material available at http://ieeexplore.ieee.org, provided by the authors.

Color versions of one or more of the figures in this article are available online at http://ieeexplore.ieee.org.

Digital Object Identifier 10.1109/TASE.2019.2963044

and crossover frequency of multiple cells. Compared to the manual method, the automated system significantly improves the efficiency of the SMC measurement.

Index Terms— Automated measurement, biological cell, optically-induced dielectrophoresis (ODEP), specific membrane capacitance (SMC).

I. INTRODUCTION

SPECIFIC membrane capacitance (SMC), defined as the electrical capacitance per unit surface area of the cell membrane, is an intrinsic electrical parameter associated with a cell's physiological state [1]. Accumulating evidence demonstrates that SMC can be a useful label-free biomarker for determining the metastatic potential, cell development stage, and degree of differentiation [2]–[4], and for distinguishing normal cells from cancerous cells [5]–[7].

Optically-induced dielectrophoresis (ODEP), which is generated by optically-induced "'virtual" electrodes and functions as optoelectronic tweezers (OETs), is a powerful technique for cell manipulation [8]–[11] and patterning of microstructures [12]–[15]. Recently, ODEP was demonstrated for quantifying the cellular SMC by manually determining a cell's crossover frequency and radius [16]–[20]. The crossover frequency of a cell is defined as the frequency of an alternating current (ac) signal at which the DEP force exerted on the cell equals zero. However, in the manual operation, several empirical trials of DEP manipulation tests must be conducted to determine the start and range of appropriate sweep frequencies. With the sweep frequency so determined, the motion of the cell is recorded throughout the sweeping process. From the recorded video, the crossover frequency and the radius of each cell are extracted and used to calculate the SMC value of each cell. All these procedures were manually executed in the previously reported ODEP systems [16], [17], [20], which were tedious and time-consuming. In addition, because the above procedures are conducted separately in the manual operation, it is difficult to synchronize the start of the frequency sweeping and the recording of cells' motion trajectories, thereby causing significant errors in the calculated crossover frequency.

In this article, we developed an automated ODEP system to improve the efficiency of the ODEP-based quantification of SMC values of cells. In addition, we developed a synchronous triggering module to control the frequency sweeping and image recording to ensure that each image sequence corresponds to the correct frequency, thereby ensuring the accuracy of the extracted crossover frequency. We also built a real-time cell identification module into

Fig. 1. Schematic of the ODEP system.

the system for visual tracking and measurement, which enables real-time (20 frames/s) quantification of multiple cells.

The automated ODEP system was utilized to measure the SMC values of three types of human urothelial cells (HUCs), including normal bladder cell line SV-HUC-1, low-grade bladder cancer cell line RT4 (grade 1, well differentiated), and high-grade bladder cancer cell line T24 (grade III, poorly differentiated). The experimental results show that the SMC value of T24 cells ($n = 45$) is significantly higher than that of RT4 cells ($n = 54$) and SV-HUC-1 cells ($n = 48$) (29.3 ± 10.4 versus 15.8 ± 3.5 mF/m^2 and 12.5 ± 2.3 mF/m^2). The quantified SMC values positively correlate with the membrane surface roughness for the three types of cells, as we measured by atomic force microscopy (AFM). Compared to the manual operation, the automated system improves SMC characterization from several minutes to a few seconds.

II. SYSTEM AND METHODS

A. Automated ODEP System

An automated ODEP system, as shown in Fig. 1, consists of an ODEP device, a signal generator (Agilent 33522A, USA) used to generate a programmable ac signal for the ODEP chip, a 3-D platform used to control the position of the ODEP chip, and a microscope (Navitar, Rochester, NY, USA) equipped with a charged coupled device (CCD; BASLER, ACA1300-30UC, Germany) for monitoring the motion of the cell and recording the manipulation process. A combination of a digital projector (Sony VPL-F600X, Japan), a personal computer with a commercial animation software program (Flash 11, Adobe, USA), and a condenser lens (Olympus, 50X, NA 0.50, WD 10.6 mm, Japan) are used to generate and project customized optical patterns. The ODEP chip comprises a photoconductive substrate, a fluidic chamber with a thickness of 70 μm for containing the cell suspension, and an

upper indium-tin-oxide (ITO)-coated glass electrode. The photoconductive electrode comprises a hydrogenated amorphous silicon layer (a-Si:H, 1 μm) deposited on an ITO-coated glass substrate via a plasma-enhanced chemical vapor deposition process. The a-Si:H film possesses intrinsic high impedance; however, its conductivity increases sharply when it is illuminated by light due to the photo-generation of electron-hole pairs. In this process, light patterns work as "'virtual' electrodes on the a-Si:H substrate. When an ac signal is applied, the "virtual" electrodes generate a nonuniform electric field in the solution and exert a DEP force on the cells therein.

To achieve the automated measurement, customized software was developed to synchronously control the ac signal, 3-D platform, and CCD camera, and enable the automated real-time measurement. The software, based on Qt (Qt Creator 4.0.3) and OpenCV 3.0, runs on a host computer with a GeForce GTX 1060 GPU.

B. Principle of SMC Quantification

The characterization of the SMC value of a cell using the ODEP device is based on the dielectric properties of the cell in a nonuniform electric field. The cells in the solution are polarized and experience a DEP force in a nonuniform ac electric field. In their suspended state during measurement, the shape of these cells was largely spherical and deviate little from the spherical shape. Thus, the spherical shell model expressed in (6) was used to interpret the experimental data [17]. To interpret the DEP force on the object with nonspherical shape (e.g., rhabditiform and ellipsoid), the more complex model [21], [22] should be employed

$$\langle F_{\text{DEP}} \rangle = 2\pi \varepsilon_m R^3 f_{\text{cm}}(f) \nabla |E_{\text{rms}}|^2 \quad (1)$$

where R represents the cell radius, ε_m denotes the permittivity of the liquid medium, E_{rms} is the root-mean-square value of the electric field, $\nabla |E_{\text{rms}}|^2$ denotes the electric field inhomogeneity, f is the frequency of the applied ac signal, and $f_{\text{cm}}(f)$ represents the real part of the Clausius–Mossotti factor, which is expressed as [23]

$$f_{\text{cm}}(f) = \frac{f^2 - f_{\text{cross}}^2}{f^2 + 2f_{\text{cross}}^2} \quad (2)$$

where f_{cross} is the DEP crossover frequency. Depending on whether the applied frequency, f, is above or below f_{cross}, the cells are acted on by a positive DEP (pDEP) force or a negative DEP (nDEP) force, respectively. Cells move toward the "virtual" electrodes when a positive force is exerted on them and move away from the "virtual" electrode when a negative force is exerted on them. Since the cell can be modeled as a homogeneous spherical cytoplasm core of radius R, surrounded by a thin membrane shell and given that the applied ac frequencies are always below 1 MHz, the SMC (i.e., C_{mem}), radius, and crossover frequency of the cell are expressed by the following equation [24]:

$$f_{\text{cross}} = \frac{\sigma_m}{\sqrt{2}\pi R C_{\text{mem}}} \quad (3)$$

where σ_m is the electrical conductivity of the liquid medium and R is the radius of cell. According to (3), the SMC value
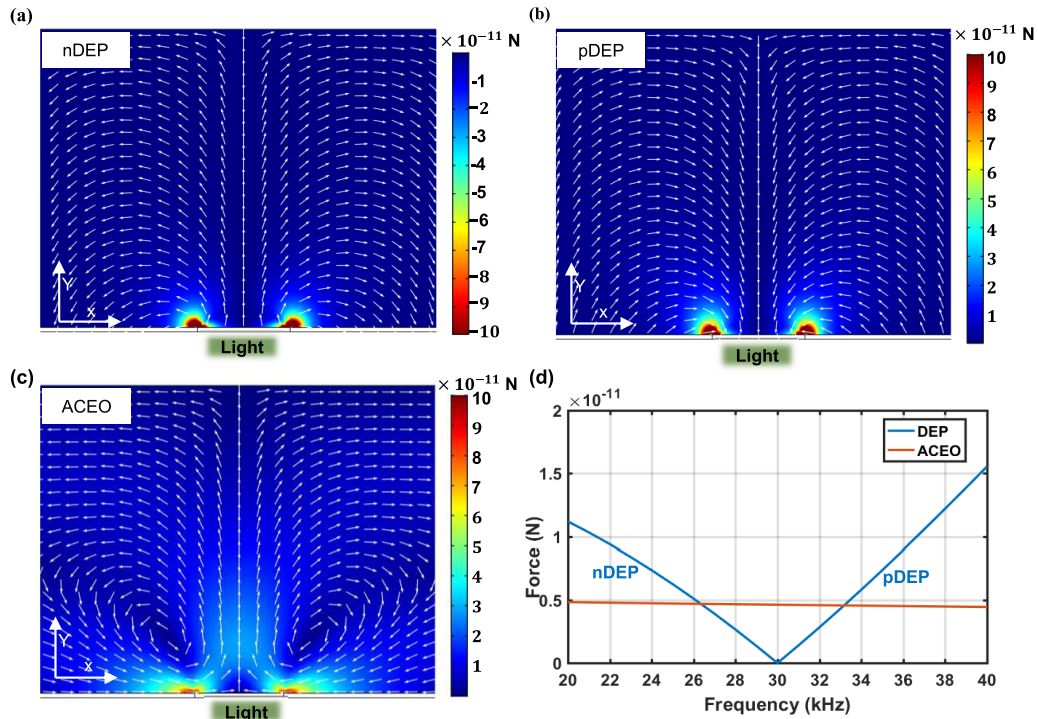
Fig. 2.   Simulation results of ACEO and DEP forces. (a) nDEP force at 20 kHz. (b) pDEP force at 40 kHz. (c) ACEO force at 20 kHz. (d) DEP and ACEO force at frequencies from 20 to 40 kHz.

of the cell can be calculated by experimentally determining the crossover frequency and the radius of the cell, demanding the development of automation techniques for accurate and efficient determination of these two parameters.

C. Determination of the Frequency-Sweeping Mode

The trajectory of cell motion depends on the mode of the sweeping frequency, which determines the value of the extracted crossover frequency. To determine the frequency-sweeping mode, i.e., from a high value to a low value or in reverse, the FEA simulation package COMSOL was used to analyze both the DEP and ac electroosmosis (ACEO) forces exerted on the cells in the ODEP chip. FEM simulation and corresponding boundary condition settings were performed by following the procedures reported in [25]. The following experimental parameters were used in the simulation: width of the light pattern $= 20\ \mu$m; height in the ODEP chip $= 70\ \mu$m; conductivity of the a-Si:H with and without illumination $= 4 \times 10^{-5}$ S/m and 1×10^{-11} S/m, respectively; conductivity of the cell suspension 1.2×10^{-2} S/m; radius of the cell $= 10\ \mu$m; relative dielectric constants of the liquid and a-Si:H $= 78$ and 11, respectively; and amplitude of the applied ac signal $= 5$ V$_{pp}$.

Equation (1) was used to calculate the DEP force. Fig. 2(a) shows the simulated distribution for the nDEP force in the solution at an ac signal frequency of 20 kHz. Fig. 2(b) shows the simulated distribution for the pDEP force in the solution at an ac signal frequency of 40 kHz. Fig. 2(c) shows the distribution of ACEO forces in the solution. The ACEO force

on the cells is given as follows [26]:

$$F_{\text{ACEO}} = -3\pi R \varepsilon_m \zeta E_t \qquad (4)$$

where ζ denotes the zeta potential, E_t denotes the tangential electric field, R is the cell radius, and ε_m denotes the permittivity of the liquid medium.

As shown in Fig. 2, the DEP and ACEO forces simultaneously exert forces on the cells in the chip. The ACEO force always drags the cells toward to the "virtual" electrode, which performs the same function as the pDEP force on the cell motion. To analyze how the ACEO force affects the motion of the cell during frequency sweep, both the DEP and ACEO forces were calculated in a frequency range of 20–40 kHz. Fig. 2(d) shows a comparison of the DEP and ACEO forces acting on the cells 10 μm above the a-Si:H film surface at the edge of the light pattern. The crossover frequency for the cell under analysis was assumed to be 30 kHz. As shown, as the frequency sweep moves from 20 to 30 kHz, the cell is acted upon by an nDEP force with an amplitude that decreases from 1.1 nN to 0, and then acted upon by an increasingly pDEP force when the frequency exceeds 30 kHz. At a frequency range from 20 to 26.2 kHz, the value of the nDEP force acting on the cell is greater than that of the ACEO force acting on it, and the cell is accelerated away from the light pattern. The velocity of the motion reaches a maximum when the nDEP force equals the ACEO force, which occurs at a frequency of ∼26.2 kHz. At a frequency range of 26.2–30 kHz, the magnitude of the ACEO force is greater than that of the nDEP force, and the cell experiences a deceleration until it stops at the farthest position. When the
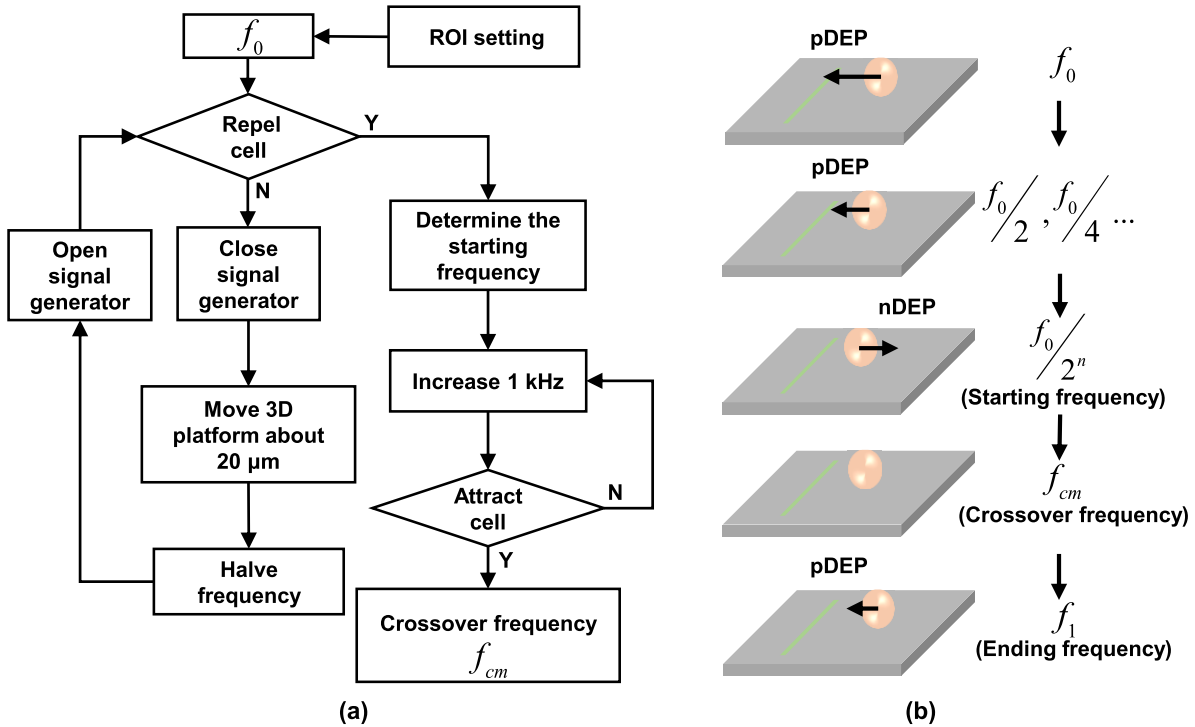
Fig. 3. Automation workflow. (a) Flowchart for determining the crossover frequency. (b) Change of cell motion during determining the starting frequency and crossover frequency.

frequency is greater than 30 kHz, the cell is acted upon by a pDEP force that has the same direction as the ACEO force, causing the cell to be accelerated toward the light pattern. As the frequency sweeps from 40 to 20 kHz, the cell is under an "attractive" motion due to the ACEO force, whereby it moves toward the light pattern and stops at the center of the pattern, at a frequency range from 40 to 26.2 kHz. Under this condition, a frequency far below the crossover frequency is required to generate an nDEP force to repel the cell, thereby the experiment cannot accurately determine the crossover frequency.

From the above discussion, the mode of the sweeping frequency must be from low to high. In this way, the cell is first repelled and then attracted again. The crossover frequency can be determined by the turning point in the motion track of the cell. In addition, Fig. 2(a)–(c) shows that the DEP force exerted on the cell decreases considerably as the cell moves far away from the light pattern. Therefore, to ensure that the DEP force is the dominant force affecting the motion of the cell, the amplitude of the applied voltage should be within 5 V_{pp} to ensure that the cell would not be repelled too far (<10 μm) away from the light pattern.

D. Automated Frequency Sweeping

The range of the sweeping frequency is a critical factor for the determination of the crossover frequency. In the traditional manual ODEP systems [16], [17], [20], the starting frequency and the frequency range were determined through numerous empirical manual trials, which is time-consuming and tedious.

Here, we developed an automated process for determining the frequency range and crossover frequency. A flowchart of the automated process is shown in Fig. 3(a). First, a region of interest containing multiple target cells is set for visual tracking of cells, and an initial frequency, f_0, is chosen to start the DEP manipulation process. f_0 is typically set in the 80–100-kHz range, which is significantly greater than the crossover frequencies of all the cells.

When an ac signal with an initial frequency is applied, cells acted on a pDEP force are attracted to the light pattern and aligned at the edge of the light pattern. This motion of cells is detected by the cell tracking algorithm in real time, which also controls the signal generator and 3-D motion stage. If an attraction motion is detected, the software turns off the signal generator, moves the 3-D stage by about 20 μm, halves the frequency, and then performs the detection again, until the cells generate a repel motion under an nDEP force. This process is also illustrated in Fig. 3(b), in which frequencies of f_0, $f_0/2$, and $f_0/4$ are successively applied until the cells are acted on a negative force at a frequency of $f_0/2^n$. The final frequency, $f_0/2^n$ is set as the starting frequency to launch a frequency-sweeping process with an increasing step of 1 kHz. The frequency-sweeping process stops after all the cells perform an attraction motion again. The final frequency, f_1, is set as the ending frequency.

For one type of cell, running the process once or twice is sufficient to determine the frequency range. Utilizing this automated process, the range of sweeping frequency for SV-HUC-1, RT4, and T24 was determined as 20–40, 10–30, and 7–20 kHz, respectively. By applying this frequency range

to the automated frequency sweeping, the crossover frequency can be extracted from motion track of the cells. Due to the real-time and quantitative analysis of the motion of the cell, the determination of frequency range and crossover frequency using the above automation process is significantly more efficient and consistent than that using the manual operation.

E. Visual Tracking of Multiple Cells

Automated visual tracking of multiple cells is critical for the extraction of cell radius, crossover frequency, and SMC value.

For this purpose, the image processing program we developed includes the functions of multicell identification for radius extraction and multicell tracking for crossover frequency determination.

For the visual tracking of cells, the first step is to identify the cells from the light pattern and image background. Considering that cells move into the optical light pattern during their motion, a green light pattern with RGB values of 0, 65, 200 was chosen as "virtual" electrode to make the cells visible even within the light pattern. The Gaussian filter was used to smooth the source image in order to decrease the optical noise caused by the projector and CCD camera. Then, the gray-scale conversion from RGB was implemented to decrease the data size to achieve a real-time image analysis. To ensure sufficient contrast of the cell relative to the light pattern and the image background, the following conversion was determined via the experimental analysis of each RGB component of the cell images:

$$G(x, y) = 0.3I_R(x, y) + 0.6I_G(x, y) + 0.1I_B(x, y) \quad (5)$$

where $G(x, y)$ represents the gray image and $I_R(x, y)$, $I_G(x, y)$, and $I_B(x, y)$ represent the red, green, and blue components of the source RGB image, respectively.

In the ODEP chip, direct binarization was found inappropriate for cell identification because both the projected light pattern and the inhomogeneous distribution of light intensity from the microscope generate large disturbances. Considering that the shapes of the cells are different from that of the light pattern, a Sobel operator [24] for extracting the horizontal gradient and vertical gradient was adopted to identify the cells from the light pattern. The edge of the light pattern was detected by the horizontal gradient, while the contour of cell was mostly extracted from the vertical gradient. Selecting a lower weight for the horizontal gradient and a higher weight for the vertical gradient can help highlight the cell contour. The horizontal weight of 0.2 and the vertical weight of 0.8 shown in (6) were experimentally determined

$$E(x, y) = 0.2|\nabla_x G(x, y)| + 0.8|\nabla_y G(x, y)| \quad (6)$$

where the $\nabla_x G(x, y)$ and $\nabla_y G(x, y)$ mean the horizontal and vertical gradients of gray image, respectively.

The adaptive binarization based on the Otsu method [27], a morphological close operation, and a contour detection based on border following algorithms [28] were subsequently conducted to achieve cell identification, as shown in Fig. 4(d)–(f).
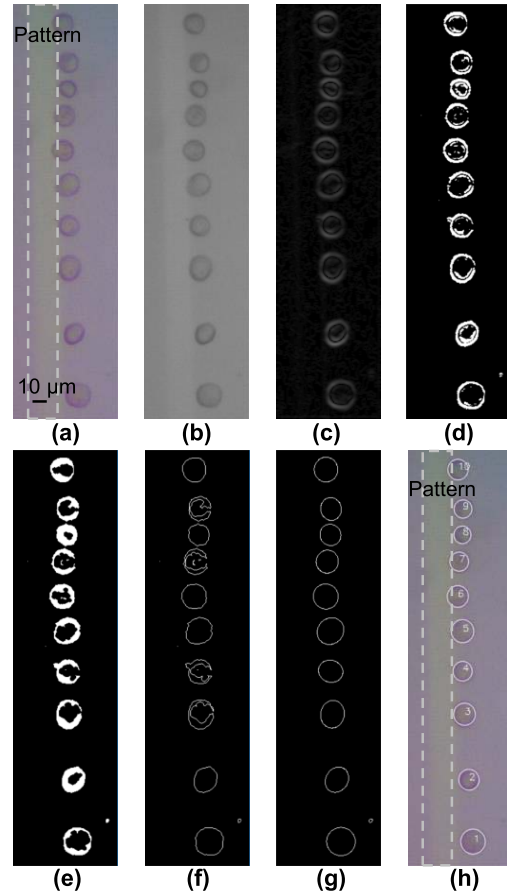
Fig. 4. Image sequence of the multicell identification (SV-HUC-1). (a) Source image. (b) Smoothed and grayed image. (c) Edge detection. (d) Adaptive binarization. (e) Morphology operation. (f) Contour determination. (g) Cell contour fitting. (h) Identified multiple cells.

For the extraction of each cell's radius, ellipses with circularity between 0.8 and 1 were chosen to fit the cell contours based on the dominant point detection algorithm [29] due to the approximately spherical shape of the cells, as shown in Fig. 4(g). The radius (R) was then calculated from the fit ellipse, according to

$$R = \frac{R_a + R_b}{2} \quad (7)$$

where R_a and R_b represent the major radius and minor radius of the ellipse. The accuracy of the measured radius directly affects the accuracy of the quantified SMC value. In our method, the repeated accuracy of fitting the cell contour was 0.5 pixel, corresponding to an accuracy of 0.2 μm for radius measurement. In addition, the real-time system measures the cell radius in each frame and uses the average radius from all the frames as the final radius for each cell, which effectively eliminates the error caused by cell rotation.

To automatically determine the crossover frequency for multiple cells, the cells must be tracked accurately. To further improve the tracking performance, a tracking algorithm based on the Kalman filter and cell ID assignment was integrated in our custom-developed software for predicting the position of each cell and tracking the multiple cells.

F. Cell Sample Preparation

Three types of HUCs were adopted as test objects to evaluate the developed system. The three types of HUCs include the immortalized normal bladder cell line SV-HUC-1, low-grade bladder cancer cell line RT4 (grade 1, well differentiated), and high-grade bladder cancer cell line T24 (grade 3, poorly differentiated). SV-HUC-1, RT4, and T24 cells were obtained from the cell bank of the Chinese Academy of Sciences, Shanghai, China, and cultured using the F-12K medium, the ATCC-formulated McCoy's 5A modified medium, and the RPMI-1640 medium, respectively, in different 25 mm^2 flasks (Corning, NY, USA). All media were supplemented with 10% fetal bovine serum and 1% penicillin (Hyclone, UT, USA). All cell lines were cultured under 37 °C and a 100% humidified atmosphere in a 5% CO^2 incubator (Thermo Fisher Scientific, Forma Series II 3110 Water-Jacketed, Waltham, MA, USA).

For quantification of the SMC, a strict experimental protocol was followed to prepare cell suspensions of T24, RT4, and SV-HUC-1. First, the cells were trypsinized, followed by the centrifugation at 1000 r/min and 4 °C for 5 min. The supernatant was discarded, and the cell precipitate retained was washed using an isosmotic fluid composed of 5% glucose and 2% bovine serum albumin (BSA). BSA was added to the isosmotic solution to prevent the cells from adhering to a-Si:H substrate. Finally, the washed cells were centrifuged and suspended in a 200-μL isosmotic solution to form a final cell suspension with an electrical conductivity of 1.2×10^{-2} S/m and a cell concentration of 10^5–10^6 cells/mL. A final cell suspension with a conductivity of 1.2×10^{-2} S/m was used in our experiments and simulation because it enables a large enough DEP force to determine the crossover frequency (see Fig. s1 in the Supplementary Material). In addition, although the isosmotic solution cannot maintain a cell viability for a long term because it can only support an osmotic pressure to avoid cell lysis but does not supply nutritional ingredients as a culture medium, the cell viability can be kept $>95\%$ in the solution within the duration of 1 h (see Fig. s2 in the Supplementary Material). Therefore, the entire cell preparation and SMC quantification process was completed within 1 h.

III. RESULTS AND DISCUSSION

The automated system was proven to be capable of simultaneously quantifying cell radius, crossover frequency, and SMC value. All the data reported here are expressed as a mean ± standard error of the mean and analyzed using the one-way ANOVA for pairwise comparison.

A. Tracking of Multiple Cells

Fig. 5(a)–(d) shows the motion of RT4 cells for a sweeping frequency ranging from 10 to 30 kHz. During the sweeping operation, the cells were first acted on by an nDEP force and moved away from the light pattern (see the Supplementary Video). Then, as the frequency increased and exceeded the crossover frequency, the cells were acted on by a pDEP force and turned back toward the light pattern. Thus, the crossover frequency for each cell was quantified according to the time
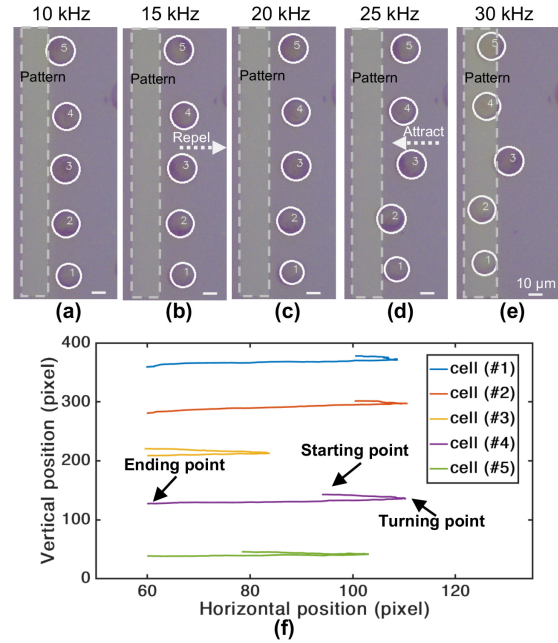
Fig. 5. Tracking results for RT4 cells. (a)–(d) Sequence of tracking results. (f) Trajectories of multiple cells.
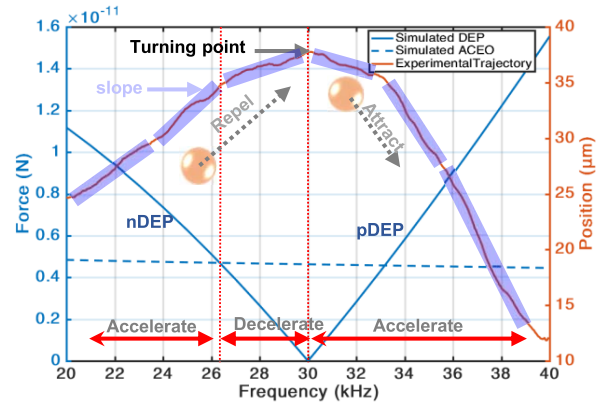
Fig. 6. Tracking trajectory compared with the simulation result.

point of the turning position. Fig. 5(f) shows the extracted trajectories for the five cells, and the frequency corresponding to the turning point was determined to be the crossover frequency. In experiments, the success rate of tracking was 100%.

To verify the accuracy of the extracted trajectories, the trajectories of the measured cells were analyzed and compared with the forces exerted on them. According to the changing slope of the trajectory of an SV-HUC-1 cell shown in Fig. 6, it can be known that the cell first moved far away from the light pattern at an increasing velocity in a frequency range of 20–26.2 kHz and then at a decreasing velocity in a frequency range of 26.2–30 kHz until it stopped. Then, the cell turned around and moved toward the light pattern at an increasing velocity as the frequency exceeded 30 kHz. The frequency corresponding to the turning point of the trajectory was 30 kHz. The force change shown by the trajectory was highly consistent with the simulated DEP and ACEO
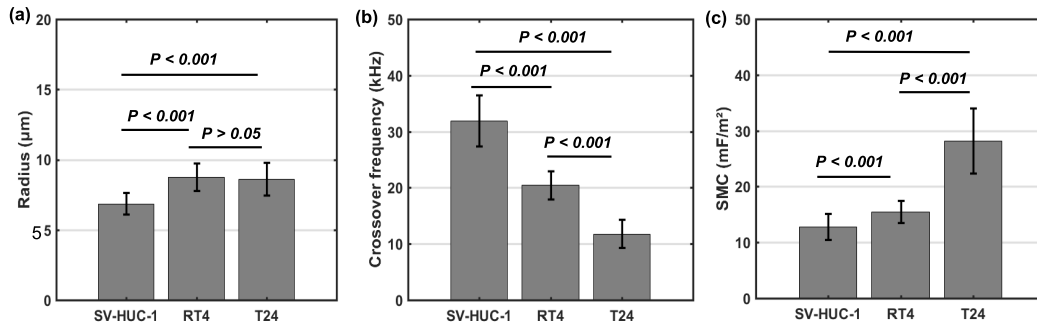
Fig. 7. Experimentally measured (a) radius, (b) crossover frequency, and (c) SMC value of SV-HUC-1, RT4, and T24 cells.

forces exerted on a cell at a crossover frequency of 30 kHz, demonstrating the accuracy of the extracted cell trajectory and quantified crossover frequency using the automated system.

B. SMC Characterization Results

The radius and crossover frequency for the SV-HUC-1, RT4, and T24 cells were quantified using the automated system. As shown in Fig. 7(a), the average radius of the SV-HUC-1 ($n = 48$), RT4 ($n = 54$), and T24 ($n = 45$) cells was 6.84 ± 0.78, 8.73 ± 0.96, and 8.6 ± 1.15 μm, respectively. Although heterogeneity existed within each type of cell, malignant urothelial cells, including RT4 and T24 cells, were significantly larger than the SV-HUC-1 cells ($P < 0.001$), which is consistent with the general finding that cancerous cells tend to have a larger radius than their normal counterparts [30], [31]. However, there was no significant difference in the cell radius between the T24 and RT4 cells ($P > 0.05$).

Fig. 7(b) shows the crossover frequencies for the three types of cells. The crossover frequency, expressed as mean $\pm$ standard error for SV-HUC-1, RT4, and T24 cells, was 31 ± 4, 20 ± 2, and 11 ± 2 kHz, respectively. The one-way ANOVA analysis showed that the crossover frequency for the three types of cells varied distinctly from each other ($P < 0.001$). The DEP crossover frequency is an overall indicator of cellular electrical conductivity and size. However, the crossover frequency is not an intrinsic property of cells since its value depends on cell radius, SMC value, and the electrical conductivity of the experimental solution surrounding the cells.

According to (3), the measured cell radius and crossover frequency were used to calculate the SMC value of each cell. As shown in Fig. 7(c), the SMC values for the SV-HUC-1, RT4, and T24 cells were 12.8 ± 2.3, 15.4 ± 2, and 28.2 ± 5.8 mF/m^2, respectively. These results demonstrate that malignant HUCs, including RT4 and T24 cells, have higher SMC values than normal HUCs. Furthermore, the SMC of high-grade malignant cells (T24) is significantly larger than that of the low-grade malignant cells (RT4) and normal urothelial cells (SV-HUC-1); however, the SMC of RT4 is only slightly larger than that of the SV-HUC-1 although the difference is still statistically significant.

The SMC value of a cell is associated with the roughness of the cell membrane. An idealized smooth lipid vesicle possesses an SMC value in the range of 4–6 mF/m^2 [32].
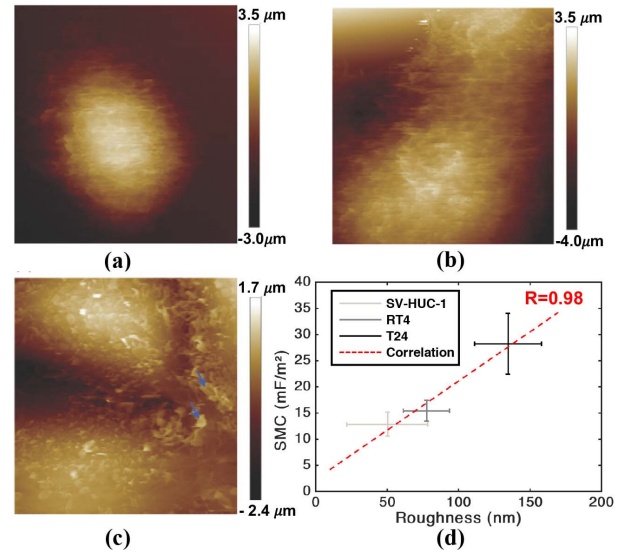
Fig. 8. AFM scanned cell membrane roughness of the three types of HUCs. (a) SV-HUC-1. (b) RT4. (c) T24. (d) Correlation between SMC and roughness.

Mammalian cells have larger SMCs than idealized smooth lipid vesicles since their membranes are less smooth [33]. Previous studies have reported that cell morphology becomes increasingly disorganized as cancer progresses, facilitating its invasion to neighboring cells and tissues [34]. In addition to the macroscopic changes in the cell morphology, cancer cells tend to grow excessive microvilli, ruffles, and folds on the cell membrane. The increase in these microscopic structures renders the cancer cells with a high SMC value and aids the cancer cells in sensing their disorganized extracellular environment [23], [35]. We performed nanoscopic imaging on the cell membranes of the three types of HUCs using AFM (Bioscope Resolve, Bruker, Santa Barbara, CA, USA) and measured their surface roughness.

Fig. 8 shows the scanned representative surface images for the three types of cells. As shown in Fig. 8, T24 cells exhibit abundant large ruffles [blue arrow in Fig. 8(c)] with a size of approximately 2–3 μm on the membrane. RT4 [see Fig. 8(b)] and SV-HUC-1 [see Fig. 8(a)] cells also exhibit microvilli and folds on their membranes, but their sizes are much smaller than those of T24 cells. Based on the scanned surface images, an rms roughness value was calculated using

TABLE I

AVERAGE TIME TAKEN BY THE AUTOMATED SYSTEM AND MANUAL
MEASUREMENT (TEN CELLS IN THIS COMPARISON)

Process	Method	Time
Frequency sweeping	Automated measurement	20 sec
	Human measurement	3.6–5.2 min
Video anylysis	Automated measurement	0.6 sec
	Human measurement	10.5–15.9 min

the commercial software, Nanoscope Analysis v1.80 (Bruker Nano Surfaces, Santa Barbara). As summarized in Fig. 8(d), the rms roughness for the three types of cells were SV-HUC-1 ($n = 4$): 50.4 ± 28.3 nm, RT4 ($n = 5$): 77.76 ± 16.18 nm, and T24 ($n = 5$): 134.8 ± 23.43 nm, respectively. The correlation coefficient between our measured SMC values and corresponding roughness values of the three types of HUC cells was 0.98, demonstrating a strong positive correlation between SMC and membrane roughness for these cells.

C. Efficiency of the Automated ODEP System

The automated ODEP system significantly outperformed the traditional manual ODEP measurement in efficiency. For SMC measurement using ODEP, the bulk time is spent on frequency-sweeping DEP forces and image analysis for calculating the cell radius and crossover frequency. In the traditional manual ODEP systems, these processes are conducted manually based on the trial and error. In the manual operation, the operator alternately adjusts the movable stage and signal generator to determine the frequency range for sweeping, and then launches the DEP force and records the video as synchronously as possible. For analyzing recorded videos, an image analysis software such as ImageJ is most often used to extract the trajectory of a cell off-line. These manual processes are time-consuming and tedious. In contrast, the automated ODEP system developed in this work automatically performed both experimental processes and image analysis in real time. The values of cell radius, crossover frequency, and SMC were obtained once the automated frequency-sweeping process was completed by the system.

Table I shows the comparison of the time taken by the automated system and by experienced human operators for quantifying the SMC values of ten RT4 cells. It costs well-trained human operators 3.6–5.2 min to record cells' frequency-sweeping motions, whereas the automated system took only 20 s. With respect to the video analysis for extracting the cell radius, crossover frequency, and SMC value, the manual process took an average of 10.5–15.9 min to characterize ten cells, whereas the automated system required almost no additional time because of its real-time image processing capability. The results prove that the automated system is capable of significantly increasing the efficiency of quantifying the SMC values of the cells.

IV. CONCLUSION

An automated and vision-feedback ODEP system was developed to quantify the cell radius, crossover frequency, and SMC value in real time. Compared to the manual process, the developed functions of the automated system, including synchronously controlling the ac signal, 3-D platform, and CCD, as well as the visual tracking of multiple cells, significantly improve the accuracy and efficiency of the SMC measurement. Experiments on malignant HUCs (RT4, T24, and SV-HUC-1) demonstrated that this automated ODEP system is an efficient tool for quantifying the electrical properties of the cells.

REFERENCES

[1] E. Neher and A. Marty, "Discrete changes of cell membrane capacitance observed under conditions of enhanced secretion in bovine adrenal chromaffin cells," *Proc. Nat. Acad. Sci. USA*, vol. 79, no. 21, pp. 6712–6716, 1982.

[2] D. R. Gossett *et al.*, "Hydrodynamic stretching of single cells for large population mechanical phenotyping," *Proc. Nat. Acad. Sci. USA*, vol. 109, no. 20, pp. 7630–7635, May 2012.

[3] E. Shojaei-Baghini, Y. Zheng, M. A. S. Jewett, W. B. Geddie, and Y. Sun, "Mechanical characterization of benign and malignant urothelial cells from voided urine," *Appl. Phys. Lett.*, vol. 102, no. 12, Mar. 2013, Art. no. 123704.

[4] J. M. Phillip *et al.*, "Biophysical and biomolecular determination of cellular age in humans," *Nature Biomed. Eng.*, vol. 1, no. 7, p. 93, 2017.

[5] Y. Zhao *et al.*, "Tumor cell characterization and classification based on cellular specific membrane capacitance and cytoplasm conductivity," *Biosensors Bioelectron.*, vol. 57, pp. 245–253, Jul. 2014.

[6] Y. Zhao *et al.*, "Single-cell electrical phenotyping enabling the classification of mouse tumor samples," *Sci. Rep.*, vol. 6, p. 19487, 2016.

[7] H. Pu *et al.*, "Micropipette aspiration of single cells for both mechanical and electrical characterization," *IEEE Trans. Biomed. Eng.*, vol. 66, no. 11, pp. 3185–3191, Nov. 2019.

[8] P. Y. Chiou, A. T. Ohta, and M. C. Wu, "Massively parallel manipulation of single cells and microparticles using optical images," *Nature*, vol. 436, no. 7049, pp. 370–372, Jul. 2005.

[9] K.-W. Huang, Y.-C. Wu, J.-A. Lee, and P.-Y. Chiou, "Microfluidic integrated optoelectronic tweezers for single-cell preparation and analysis," *Lab Chip*, vol. 13, no. 18, p. 3721, 2013.

[10] T.-K. Chiu *et al.*, "Optically-induced-dielectrophoresis (ODEP)-based cell manipulation in a microfluidic system for high-purity isolation of integral circulating tumor cell (CTC) clusters based on their size characteristics," *Sens. Actuators B, Chem.*, vol. 258, pp. 1161–1173, Apr. 2018.

[11] S. Zhang *et al.*, "Patterned optoelectronic tweezers: A new scheme for selecting, moving, and storing dielectric particles and cells," *Small*, vol. 14, no. 45, Nov. 2018, Art. no. 1803342.

[12] N. Liu *et al.*, "3-D non-UV digital printing of hydrogel microstructures by optically controlled digital electropolymerization," *J. Microelectromech. Syst.*, vol. 24, no. 6, pp. 2128–2135, Dec. 2015.

[13] N. Liu *et al.*, "Extracellular-controlled breast cancer cell formation and growth using non-UV patterned hydrogels via optically-induced electrokinetics," *Lab Chip*, vol. 14, no. 7, p. 1367, 2014.

[14] M. Li *et al.*, "Performance investigation of multilayer MoS_2 thin-film transistors fabricated via mask-free optically induced electrodeposition," *ACS Appl. Mater. Interfaces*, vol. 9, no. 9, pp. 8361–8370, Mar. 2017.

[15] N. Liu *et al.*, "Rapidly patterning micro/nano devices by directly assembling ions and nanomaterials," *Sci. Rep.*, vol. 6, p. 32106, Aug. 2016.

[16] W. Liang, K. Zhang, X. Yang, L. Liu, H. Yu, and W. Zhang, "Distinctive translational and self-rotational motion of lymphoma cells in an optically induced non-rotational alternating current electric field," *Biomicrofluidics*, vol. 9, no. 1, Jan. 2015, Art. no. 014121.

[17] W. Liang, Y. Zhao, L. Liu, Y. Wang, W. J. Li, and G.-B. Lee, "Determination of cell membrane capacitance and conductance via optically induced electrokinetics," *Biophys. J.*, vol. 113, no. 7, pp. 1531–1539, Oct. 2017.

[18] W. Liang, Y. Wang, H. Zhang, and L. Liu, "Characterization of the self-rotational motion of stored red blood cells by using optically-induced electrokinetics," *Opt. Lett.*, vol. 41, no. 12, p. 2763, Jun. 2016.

[19] F. H. Labeed, H. M. Coley, and M. P. Hughes, "Differences in the biophysical properties of membrane and cytoplasm of apoptotic cells revealed using dielectrophoresis," *Biochim. Biophys. Acta (BBA)-Gen. Subjects*, vol. 1760, no. 6, pp. 922–929, 2006.

[20] Y. Lin *et al.*, "SMC difference of normal and cancerous human urothelial cells quantified with an opto-electrokinetic device," in *Proc. Int. Conf. Manipulation, Autom. Robot. Small Scales (MARSS)*, Jul. 2018, pp. 1–5.

[21] H. Morgan and N. G. Green, "Dielectrophoretic manipulation of rod-shaped viral particles," *J. Electrostatics*, vol. 42, no. 3, pp. 279–293, Dec. 1997.

[22] T. Kakutani, S. Shibatani, and M. Sugai, "Electrorotation of non-spherical cells: Theory for ellipsoidal cells with an arbitrary number of shells," *Bioelectrochem. Bioenergetics*, vol. 31, no. 2, pp. 131–145, Jul. 1993.

[23] P. Gascoyne and S. Shim, "Isolation of circulating tumor cells by dielectrophoresis," *Cancers*, vol. 6, no. 1, pp. 545–579, Mar. 2014.

[24] K. L. Chan, P. R. C. Gascoyne, F. F. Becker, and R. Pethig, "Electrorotation of liposomes: Verification of dielectric multi-shell model for cells," *Biochim. Biophys. Acta (BBA)-Lipids Lipid Metabol.*, vol. 1349, no. 2, pp. 182–196, 1997.

[25] W. Liang *et al.*, "Simultaneous separation and concentration of micro- and nano-particles by optically induced electrokinetics," *Sens. Actuators A, Phys.*, vol. 193, pp. 103–111, 2013.

[26] A. Castellanos, A. Ramos, A. Gonzalez, N. G. Green, and H. Morgan, "Electrohydrodynamics and dielectrophoresis in microsystems: Scaling laws," *J. Phys. D, Appl. Phys.*, vol. 36, no. 20, pp. 2584–2597, Oct. 2003.

[27] N. Otsu, "A threshold selection method from gray-level histograms," *IEEE Trans. Syst., Man, Cybern.*, vol. 9, no. 1, pp. 62–66, Jan. 1979.

[28] S. Suzuki and K. Abe, "Topological structural analysis of digitized binary images by border following," *Comput. Vis., Graph., Image Process.*, vol. 29, no. 3, p. 396, Mar. 1985.

[29] C.-H. Teh and R. Chin, "On the detection of dominant points on digital curves," *IEEE Trans. Pattern Anal. Mach. Intell.*, vol. 11, no. 8, pp. 859–872, Aug. 1989.

[30] W.-P. Chou *et al.*, "The utilization of optically-induced-dielectrophoresis (ODEP)-based virtual cell filters in a microfluidic system for continuous isolation and purification of circulating tumour cells (CTCs) based on their size characteristics," *Sens. Actuators B, Chem.*, vol. 241, pp. 245–254, Mar. 2017.

[31] F. Yang *et al.*, "Dielectrophoretic separation of colorectal cancer cells," *Biomicrofluidics*, vol. 4, no. 1, Mar. 2010, Art. no. 013204.

[32] H. Liu *et al.*, "Biophysical characterization of bladder cancer cells with different metastatic potential," *Cell Biochem. Biophys.*, vol. 68, no. 2, pp. 241–246, Mar. 2014.

[33] S. H. Donaldson, M. Valtiner, M. A. Gebbie, J. Harada, and J. N. Israelachvili, "Interactions and visualization of bio-mimetic membrane detachment at smooth and nano-rough gold electrode surfaces," *Soft Matter*, vol. 9, no. 21, pp. 5231–5238, 2013.

[34] S. Moritani *et al.*, "Topographical, morphological and immunohisto-chemical characteristics of carcinoma in situ of the breast involving sclerosing adenosis. Two distinct topographical patterns and histological types of carcinoma in situ," *Histopathology*, vol. 58, no. 6, pp. 835–846, May 2011.

[35] P. R. C. Gascoyne, J. Noshari, F. F. Becker, and R. Pethig, "Use of dielectrophoretic collection spectra for characterizing differences between normal and cancerous cells," *IEEE Trans. Ind. Appl.*, vol. 30, no. 4, pp. 829–834, Jul./Aug. 1994.